AD-A261 355

MENTATION PAGE

Form Approved
OMB No. 0704-0188

REPORT DATE	3. REPORT TYPE AND DATES COVERED
2/93	FINAL 10/1/90-11/30/91

4. TITLE AND SUBTITLE
Wind-driven Coastal Generation of Annual Mesoscale Eddy Activity in the California Current

5. FUNDING NUMBERS
N00014-91-J-1278

6. AUTHOR(S)
Alejandro Pares-Sierra, Warren B. White, C-K Tai

7. PERFORMING ORGANIZATION NAME(S) AND ADDRESS(ES)
University of California, San Diego
Scripps Institution of Oceanography
La Jolla, CA 92093-0230

8. PERFORMING ORGANIZATION REPORT NUMBER

9. SPONSORING/MONITORING AGENCY NAME(S) AND ADDRESS(ES)
Office of Naval Research
800 North Quincy Street
Arlington, VA 22217-5000

10. SPONSORING/MONITORING AGENCY REPORT NUMBER

11. SUPPLEMENTARY NOTES
Manuscript entitled " Wind driven coastal generation of annual meso-scale eddy activity in California Current".Prepared in co-operation with C.-K. Tai

12a. DISTRIBUTION/AVAILABILITY STATEMENT
Published in J. Physical Oceanography 1993.

12b. DISTRIBUTION CODE

13. ABSTRACT *(Maximum 200 words)*

ABSTRACT

Two candidate sources for the generation of mesoscale eddy activity in the California Current are local baroclinic instability and/or the wind stress adjacent to the coast. The latter constitutes remote forcing with eddy activity propagating westward from the coast into California Current via Rossby wave dynamics. In this study, two wind-driven models are utilized to test the relative significance of these two sources. One is an eddy resolving quasigeostrophic (QG) model, with the ability to represent baroclinic instability but not the coastal response to winds. The other is a 1 1/2-layer primitive equation (PE) model with the ability to represent the coastal response to winds but not baroclinic instability. Both models have the same spatial grid (i.e.. approximately 20 km) and are driven by the same coarse-grid wind stress forcing fields over the same one year time period (i.e. January 1987 to December 1987). The PE model is able to simulate qualitatively this distribution of the eddy variance as it appears in altimetric sea level, yielding significant coherence and phrase between model and observed sea-level residuals along longitude/time matrices at 30°N and 40°N. The QG model on the other hand, is found incapable of simulating the main features of this distribution of eddy variance.

14. SUBJECT TERMS
Coastal circulation, California Current

15. NUMBER OF PAGES
12 pp

16. PRICE CODE

17. SECURITY CLASSIFICATION OF REPORT	18. SECURITY CLASSIFICATION OF THIS PAGE	19. SECURITY CLASSIFICATION OF ABSTRACT	20. LIMITATION OF ABSTRACT
unclassified	unclassified	unclassified	SAR

Wind-driven Coastal Generation of Annual Mesoscale Eddy Activity in the California Current

ALEJANDRO PARES-SIERRA*,+ WARREN B. WHITE*, AND C.-K. TAI**

*Scripps Institution of Oceanography, UCSD, La Jolla, California
+Centro de Investigación Científica y Educación Superior de Ensenada
**NOAA, NOS, Rockville, Maryland

(Manuscript received 26 September 1991, in final form 7 May 1992)

ABSTRACT

Two candidate sources for the generation of mesoscale eddy activity in the California Current are local baroclinic instability and/or the wind stress adjacent to the coast. The latter constitutes remote forcing, with eddies propagating westward from the coast into the California Current via Rossby wave dynamics. In this study, two wind driven models are utilized to test the relative significance of these two sources, one an eddy resolving quasi- geostrophic (Q-G) model, which has the ability to represent baroclinic instability but not the coastal response to winds, and the other a 1-1/2 layer primitive equation (PE) model, which has the ability to represent the coastal response to winds but not baroclinic instability. Both models have the same spatial grid (i.e., approximately 20 km) and are driven by the same course-grid wind stress forcing fields over the same one year time period (i.e., November 1986 to October 1987), this period chosen because of the availability of Geosat altimetric sea level observations with which to verify these models. Earlier, White *et al.* (1990) analysed these same altimetric sea level observations, finding dominant mesoscale eddy activity occurring on wavelength scales of 400-800 km and period scales of 6-12 months, propagating to the west at 2-5 cm/sec, faster at lower latitude, governed by Rossby wave dynamics. We find in this study that the PE model is able to simulate qualitatively this distribution of the eddy variance as it appears in altimetric sea level, yielding significant coherence and phase between model and observed sea level residuals along longitude/time matrices at 30°*N* and 40°*N*. The Q-G model, on the other hand, is found incapable of simulating even the qualitative distribution of eddy variance. The reason for the agreement between the PE model and the satellite altimetric sea level observations is that the dominant source of mesoscale eddy activity on these time and space scales is the wind forcing adjacent to the coast, modified by both Rossby and Kelvin wave dynamics.

1. Introduction

Mesoscale eddy activity in the California Current system has been examined repeatedly over the years (e.g., Wyllie 1966; Bernstein et al. 1977; Simpson et al. 1984; Reinecker et al. 1987) using both in situ and satellite observations. The study of eddy activity in the California Current began with the analysis of in situ hydrographic data collected during a sequence of CALCOFI cruises beginning in 1950, with eddies and fronts embedded in the California Current repeatedly observed over a period of many years. In long-term monthly mean dynamic height maps from CALCOFI, Wyllie (1966) demonstrated the existence of semipermanent eddies in the California Current off Point Conception and adjacent to Punta Eugenia. Hickey (1979) later demonstrated the existence of a semipermanent eddy west of Monterey in these same data. Prior to satellite observations, transient eddy activity was difficult to study with the CALCOFI hydrograph observations because of lack of adequate time sequences that would allow individual eddies to be tracked over space-time. The advent of satellite observations made possible a synoptic view of the surface eddy field, often repeated for weeks and months at a time.

Transient eddy activity in the California Current was first studied using AVHRR observations by Bernstein et al. (1977), finding transient mesoscale eddy activity in the California Current to have originated in near-coastal waters. This observation was followed by Owen (1980) who examined mesoscale eddy activity in the California Current from a variety of in situ and satellite observations, finding semipermanent eddies associated with coastal and bathymetric irregularities (e.g., the semipermanent eddy off Point Conception), and transient eddies associated with wind events adjacent to the coast. A thorough hydrographic study of one specific transient eddy observed in satellite data was conducted by Simpson et al. (1984), in which its origin was examined in the light of theories of topographic generation and baroclinic instability. This eddy was

Corresponding author address: Alejandro Pares-Sierra, Scripps Institution of Oceanography, A-021, University of California, 95 Gilman Drive, La Jolla, CA 92093-0221.

found to have coastal undercurrent water at its center, suggesting its origin at the coast. These satellite studies began to suggest that transient mesoscale eddy activity in the California Current had its origin in the near coastal region, propagating westward from there into the current.

A sequence of localized intensive hydrographic surveys in a small subregion of the California Current region was conducted (called OPTOMA) in order to study the behavior of mesoscale eddy activity in the current (e.g., Robinson et al. 1986; Reinecker et al. 1987). The high-resolution data of the OPTOMA experiment was inserted by Reinecker et al. (1987) into a quasigeostrophic numerical model, performing dynamical interpolation and providing forecasts of the eddy evolution in the survey region. They found these mesoscale eddies tracking westward through the subregion at Rossby wave speeds. Based on an analysis of the energy budget, they found that forcing by the curl of the wind stress, as well as baroclinic instability processes, were essential for understanding the evolution of the observed eddies in the current. This work had little to say about the origin of these eddies, focusing rather on their modification by the local wind-stress curl and the background current.

Mesoscale eddy activity over the entire California Current region was examined by White et al. (1990), based upon altimetric sea-level observations from the Geosat Exact Repeat Mission (ERM) over the one-year period from January 1987 to December 1987. Analysis of sea-level residuals from the long-term mean permitted a visualization of the space–time evolution of the mesoscale eddy activity over the entire region not previously possible. The rms differences of the altimetric sea level about the mean showed maximum eddy activity at three principal locations adjacent to the coast of California; that is, off Punta Eugenia at 27°N, southwest of Point Conception at 32°N, and adjacent to the coast between Monterey and Cape Mendocino. Time–longitude plots demonstrated coastal mesoscale eddy activity propagating westward into and through the California Current.

Numerical models are powerful tools in the investigation of mesoscale eddy generation and dynamics. A good example of this is given by Holland and Lin (1975a,b) and Holland (1978), who used both quasigeostrophic (QG) and primitive equation (PE) models in studying the role of mesoscale eddies in the general circulation of the ocean. Holland established that mesoscale eddies spontaneously arise from instabilities in the mean ocean currents and are subsequently controlled by nonlinear Rossby wave dynamics. Recently, numerical models have developed the capability for conducting realistic simulations that allow this and other hypotheses to be tested. A particularly relevant modeling study of the variability of the eastern Pacific is the one done by Cummins et al. (1986) using a simplified one-layer QG model. They analyzed the simulated Rossby wave field in the eastern Pacific and found it to be dominated by waves emanating from the eastern boundary, organized into coherent patterns. This showed very clearly that variable wind curl near the coast can be a source for Rossby waves for the whole eastern Pacific. The model used in this latter study does not have the capacity of becoming baroclinicly unstable (being a one-layer model) and hence, could not assess the importance of this contribution to the overall eddy energy budget of the region. More recent studies (e.g., Auad et al. 1991) have shown that for the QG model in general the contribution to the eddy variability in the California Current region from the wind-curl forcing is overshadowed by the contribution from baroclinic instability.

Therefore, two sources for the generation of mesoscale eddy activity in the California Current are hypothesized: i.e., local baroclinic instability of the main current and remote generation of eddy activity by the wind stress adjacent to the coast, the latter propagating westward into (and through) the California Current via Rossby wave dynamics. To test these hypotheses, two numerical models are utilized. One model is eight layers, eddy resolving, and quasigeostrophic (QG), with the ability to represent baroclinic instability but not the coastal response to winds. The other model is a 1½-layer primitive equation (PE), with the ability to represent the coastal response to winds but not baroclinic instability. Both numerical models have a similar spatial grid (i.e., approximately 20 km) and are driven by the same coarse-grid wind stress forcing fields over the same one-year time period (i.e., January 1987 to December 1987). Each model attempts to provide a realistic simulation of the mesoscale eddy activity in the California Current. These model results are then compared with those observed during the last year of the Geosat ERM (White et al. 1990), testing the eddy generation mechanism isolated in each model. Of course, each of these models (QG and PE) include "more physics" than just baroclinic instability and local wind forcing at the coast. However, as argued below, for the California Current area and for the realistic wind used, those two mechanisms dominate the response of the QG and PE model, respectively.

2. Geosat altimetric sea-level residuals in the California current

Geosat altimetric sea-level residuals in the California Current region for the period January 1987 to December 1987 are used in this study in a comparison with the model-generated mesoscale eddy activity. A complete description of the Geosat Exact Repeat Mission (ERM) in this region is given by White et al. (1990); in this study, only a brief account of the ERM and the extensive preprocessing of the raw data is given. This is followed by a discussion of the rms of the intra-annual variability about the 1987 mean, taken from White et al. (1990).

The Geosat ERM has a 17-day repeat orbit cycle and a longitudinal track separation of approximately

1.47 degrees. Along the ground track, one-second averages of altimetric sea-level measurements are formed with a spatial resolution of approximately 6.7 km. The grid resulting from the superposition of all the ascending and descending orbits in the California Current region is shown in Fig. 1. A one-year period (from January 1987 to December 1987) is available for use in this study, previously analyzed by White et al. (1990). Preprocessing of the altimetric sea-level observations begins with an application of the environmental corrections supplied with the raw observations. Next, to remove the geoid and residual orbit error, the track mean is subtracted from each individual observation, producing altimetric sea-level residuals, and the resulting residuals are detrended along each track. A Gaussian filter is then applied to the alongtrack altimetric sea-level residuals, suppressing the variance of wavelengths less than 50 km. This latter procedure is conducted as a quality control exercise to suppress white noise assumed to be of instrumental origin. Finally, the alongtrack data is decimated at 25-km intervals. Only the filtered/decimated altimetric sea-level residuals along ascending tracks are used in this study.

These filtered/decimated altimetric sea-level residuals are mapped onto a regular 0.5° latitude–longitude grid (White et al. 1990) over the California Current region every 17 days over the one-year period of interest. The subsequent spatial distribution of rms differences about the one-year mean is displayed in Fig. 2. Overall, maximum rms variability is confined to the coastal ocean in three different latitude locations. A latitude maximum occurs adjacent to the coast of Northern California from 37°N to 40°N, extending

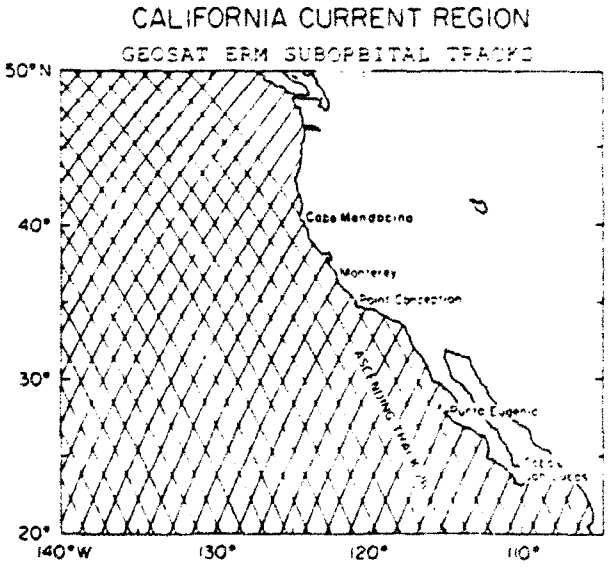

FIG. 1. Distribution of the ascending and descending tracks from the GEOSAT Exact Repeat Mission. Each track was separated from adjacent tracks by approximately 140 km; each track was repeated every 17 days for the one-year period (January 1987–December 1987) of this study.

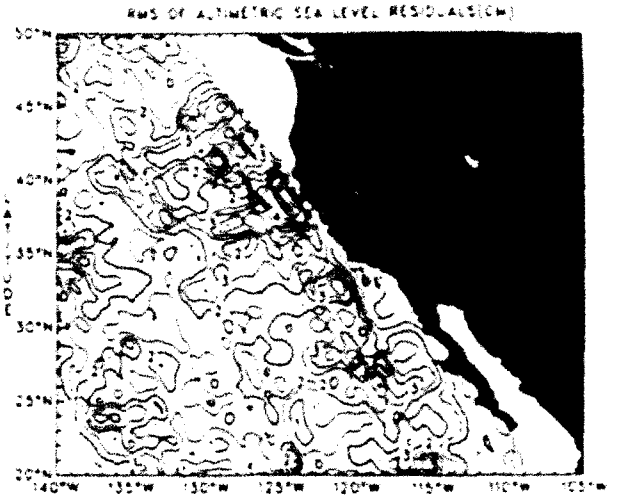

FIG. 2. Observed spatial distribution of the rms residuals of Geosat altimetric sea level about the one-year mean from January 1987–December 1987.

from Monterey to Cape Mendocino. Another local maximum occurs southwest of Point Conception near 32°N, 120°W, where frequent mesoscale eddy activity (i.e., the Southern California Eddy) was noted repeatedly (e.g., Simpson et al. 1986). A third local maximum occurs directly west of Punta Eugenia where frequent mesoscale eddy activity was also noted earlier (e.g., Wyllie 1966). Most importantly with regards to this study are the extensions of these rms variability maxima toward the west, suggesting westward propagation of mesoscale eddy energy from these apparent source regions, each extending from the coast out into the California Current itself.

3. Primitive equation model of the California current

The 1½ layer PE model used in this study is described in detail by Pares-Sierra and O'Brien (1989). It consists of one dynamically active layer of constant density ρ and variable depth H over an infinitely deep lower layer of higher density $\rho + \Delta\rho$. The model domain extends from 20°–50°N and from the coast of North America to 150°W. The eastern boundary of the model domain realistically follows the geometry of the eastern North Pacific coastline. The northern, southern, and western boundaries are open, with a Sommerfeld radiation condition (e.g., Camerlengo and O'Brien 1980) imposed there. The spatial resolution over this model domain is approximately 20 km in both the zonal and meridional directions. The equations of the model are

$$\frac{\partial U}{\partial t} + \frac{1}{a\cos\theta}\frac{\partial}{\partial\phi}\left(\frac{U^2}{H}\right) + \frac{1}{a}\frac{\partial}{\partial\theta}\left(\frac{UV}{H}\right) - (2\Omega\sin\theta)V$$

$$= \frac{-g'}{2a\cos\theta}\frac{\partial H^2}{\partial\phi} + \frac{\tau^\phi}{\rho} + A\nabla^2 U$$

$$\frac{\partial V}{\partial t} + \frac{1}{a\cos\theta}\frac{\partial}{\partial\phi}\left(\frac{UV}{H}\right) + \frac{1}{a}\frac{\partial}{\partial\theta}\left(\frac{V^2}{H}\right) + (2\Omega\sin\theta)U$$
$$= \frac{-g'}{2a}\frac{\partial H^2}{\partial\theta} + \frac{\tau^\theta}{\rho} + A\nabla^2 V$$

$$\frac{\partial H}{\partial t} + \frac{1}{a\cos\theta}\left[\frac{\partial U}{\partial\phi} + \frac{\partial}{\partial\theta}(V\cos\theta)\right] = 0,$$

where θ and ϕ are the latitude and longitude, respectively; U and V are the transports in the east–west and north–south directions, respectively; H is the depth of the upper layer; g' is reduced gravity; τ^ϕ and τ^θ are the wind-stress components; A is the eddy viscosity coefficient; and a is the radius of the earth. The values of the parameters are given in appendix A.

Earlier, Pares-Sierra and O'Brien (1989) had forced this model with realistic monthly mean wind stress (i.e., computed from the COADS surface wind observation set), to simulate the interannual variability of the California Current. The pattern of the average circulation in the North Pacific derived from the 1½ layer PE model was demonstrated to be similar to that observed. Moreover, upper-layer seasonal and interannual variability in the model was demonstrated to be similar to that observed at a number of coastal sea level stations (Pares-Sierra and O'Brien 1989). At that time, Pares-Sierra and O'Brien (1989) found most of the seasonal variability in the model originating at or near the coast. Subsequent off-shore propagation of this coastal variability appeared to provide for significant mesoscale eddy activity in the California Current (Pares-Sierra 1991). This supported the earlier suggestion by Mysak (1983) that annual fluctuations at the eastern boundary were responsible for most of the mesoscale eddy activity in the interior ocean.

In the present study, the Fleet Numerical Oceanographic Center (FNOC) Surface Wind Analyses are used to compute synoptic wind-stress estimates for driving the PE model over the period coincident with the Geosat ERM. The synoptic FNOC wind-stress estimates have a resolution of two degrees in the meridional and zonal directions, and of one day in time; these estimates are interpolated down onto the 10 km–20 minute space–time grid, upon which the model is integrated. The model integration is conducted in three stages: the model is driven from rest for 10 years with the annual mean wind-stress estimates; then, the model is driven for another ten years with the long-term mean annual cycle of the wind stress; finally, the model is driven for ten years from 1978 to 1987 with the synoptic wind-stress estimates. Model results from the final year (i.e., January 1987–December 1987) are compared with the Geosat altimetric sea-level observations.

Earlier, Pares-Sierra and O'Brien (1989) demonstrated that the large-scale features of the California Current at the sea surface can be simulated in qualitative fashion with a wind-driven reduced gravity 1½ layer PE model. This is demonstrated in the upper panel of Fig. 3, where the mean upper-layer thickness distribution from the PE model over the California Current region is displayed. In this mean distribution, the eastern limb of the subtropical gyre can be seen driven by the mean large-scale anticyclonic wind-stress curl over the North Pacific. The southward flow that constitutes this portion of the subtropical gyre is the California Current, found to occur 250–750 km off the coast of California, tending into the coast as the current nears northern Mexico (i.e., Baja California). Off the coast of California, the current is well separated from the coastal waveguide by a trough in sea level that occurs 100–200 km offshore. Inshore of this trough, the increase of sea level toward the coast indicated the

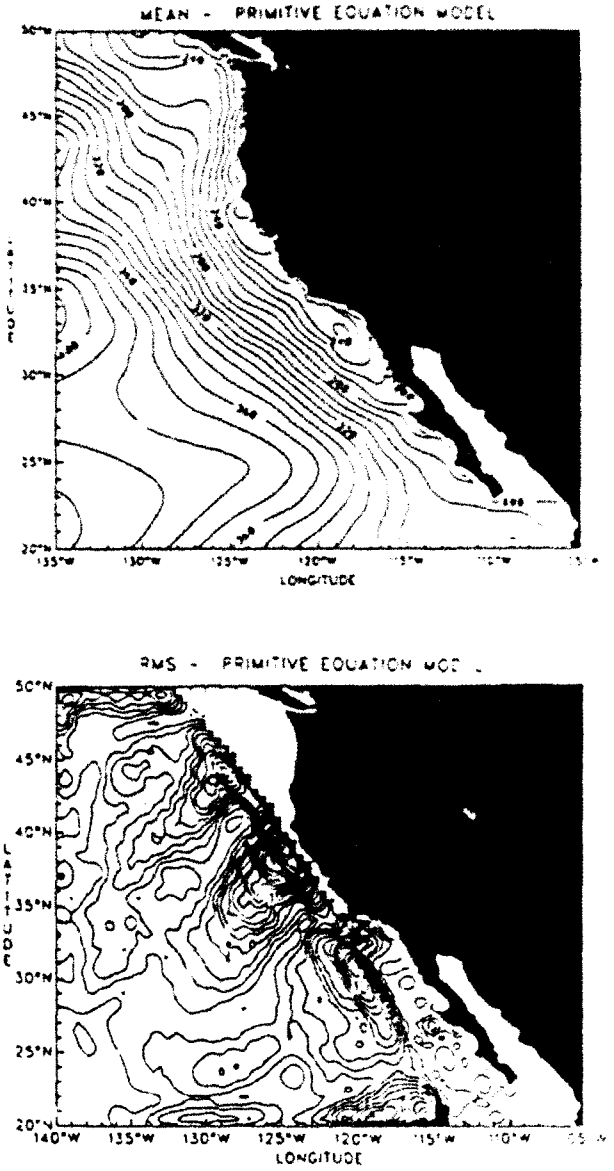

FIG. 3. (Upper panel) Spatial distribution of the mean upper-layer thickness (m) obtained from the wind-driven 1½ layer PE model for the one-year period January 1987–December 1987. (Lower panel) Spatial distribution of the rms residuals (cm) of the PE model sea level for the one-year period January 1987–December 1987.

presence of a coastal countercurrent, sometimes called the Davidson Current. The Davidson Current is strongest in winter along the northern portion of the California coast. The California Current is seen to be well separated from the coast of California; hence, the two sources of mesoscale eddy activity to be examined in this study (i.e., baroclinic instability and coastal wind generation) are also seen to be separated geographically.

In the PE model, the location of maximum variability in response to synoptic FNOC wind-stress forcing is not in the California Current itself but in the waveguide adjacent to the coast of California. This can be seen in the lower panel of Fig. 3, where the spatial distribution of the rms of sea-level residuals is displayed. Overall, the maximum rms variability is confined to the coastal ocean in two different latitude locations. A latitude maximum occurs adjacent to the coast of Northern California from 37° to 40°N, extending from Monterey to Cape Mendocino, very similar to that observed in Fig. 2. Another local maximum occurs southwest of Point Conception, where intense variability is observed in the local wind-stress field east of the Channel Islands. These areas of enhanced mesoscale variability coincide with those found by Cummins et al. (1986). Most important are the extensions of the two rms variability maxima in Fig. 3 toward the southwest, consistent with that observed in Fig. 2 and, again, suggestive of westward propagation from the coast into the California Current located in the offshore region.

This rms distribution is the result of an annual pattern of upwelling and downwelling associated with the annual north–south reversal of the wind stress along the coast. Superimposed on this are the upwelling/downwelling events associated with synoptic changes in wind-stress forcing; these synoptic events, however, are generally much smaller than those associated with the annual cycle of wind-stress variability. The latter results from a deepening (weakening) of the semipermanent continental thermal low over California during spring–summer (autumn–winter), which generates strong northwesterly (weak northwesterly) wind stress parallel to the coast. Strong northwesterly wind stress is upwelling favorable, represented in the PE model by a reduction in the depth of the upper layer. Weak northwesterly wind stress along the southern part of the domain, and a reversal of the direction of the wind stress in the vicinity of Cape Mendocino, during autumn–winter weakens the upwelling pattern. This is interspersed with regions of coastal downwelling. Seasonal coastal variability is strongest in the vicinity of Cape Mendocino, where an actual seasonal wind-stress reversal is present, with a secondary maximum occurring southwest of Point Conception.

4. Eddy-resolving quasigeostrophic model of the California current

A quasigeostrophic (QG) eddy-resolving model (Holland and Vallis 1990) is used to investigate the role of baroclinic instability as a mechanism for generating mesoscale eddy activity in the California Current. Details of the physics of this model can be found in Holland (1978), and discussion of similarities and differences between multilayer QG and PE models is conducted in Holland (1985, 1986). The same model is used by Auad et al. (1991) to study the circulation and energetics of the eastern Pacific from the point of view of QG dynamics. The equations of the model are

$$\frac{DQ_k}{Dt} = \frac{\nabla \times \tau}{\rho_0 H_k}\delta_{k,1} + A_H\nabla^4\psi_k - \epsilon\nabla^2\psi_k\delta_{k,n},$$

where

$$Q_k = \nabla^2\psi_k + f_0 + \frac{f_0}{H_k}(h_{k+1/2} - h_{k-1/2}) + \frac{f_0 b}{H_k}\delta_{k,n}$$

is the QG potential vorticity for the kth layer ($k = 1, 8$). Here $\nabla \times \tau$ is the wind-stress curl, ρ_0 is the reference density of the fluid, H_k is the kth layer thickness; $\delta_{i,j}$ is a Kronecker delta, A_H is the lateral friction coefficient, ψ_k is the total streamfunction for the kth layer, ϵ is the bottom friction coefficient, f_0 and β are the Coriolis parameter and its meridional gradient, respectively, taken at the model central latitude ($y_c = 33°$N; $b(x, y)$ is the bottom topography. The total derivative operator is $D/Dt = \partial/\partial t + J(\psi_k, (\ ))$, where the last term is the Jacobian operator. The $h_{k+1/2}$ symbol represents the vertical displacement of the $(k + 1/2)$th interface, which can be regarded as an isopycnal surface:

$$h_{k+1/2} = \frac{f_0}{g'_{k+1/2}}(\psi_k - \psi_{k+1}),$$

where $g'_{k+1/2}$ is the reduced gravity corresponding to the $(k + 1/2)$th interface. An important characteristic of this model, in regard to the present study, is the form that the boundary condition takes in terms of the primary field ψ. The boundary condition imposed at the lateral boundaries is that of no normal flow, that is,

$$n \cdot V = 0 \Rightarrow \psi = \text{const} \quad \text{at the boundary;}$$

in particular, the depth of the upper layer ($h \propto \psi_1 - \psi_3$) is constant along the boundary (but a function of time) (Holland 1978). The method for solving these equations has been given in many papers (e.g., Holland 1978; Cummins and Mysak 1988; Holland and Vallis 1990).

This QG model extends over the same domain as the PE model (i.e., 20°–50°N, coast of North America–150°W), with approximately the same space–time grid resolution and with eight layers in the vertical.

Many earlier studies using this QG model concentrate upon simulating mesoscale eddy activity in the very energetic western boundary currents (e.g., Schmitz and Holland 1986). In the study of the California Current, a different set of model parameters is chosen, requiring the model to simulate eastern boundary current variability with much greater vertical resolution in the

upper 500 m of ocean and with less density contrast between layers. The model parameters used in this study are given in appendix B. The reduced gravity estimates are based on historical CalCOFI hydrographic observations taken near the California coast.

Integration of this eddy-resolving QG model occurs in step-wise fashion similar to that used in integrating the PE model. The mean wind-stress curl used to force the model is computed from the FNOC Surface Wind Analysis extending for nearly 10 years from 1977 to 1987. The QG model is integrated from rest using the annual cycle of monthly mean wind-stress curl until statistical equilibrium is reached; then the model is driven through three cycles of the 7-year synoptic wind-stress curl. During the last year of this integration (January–December 1987), QG model upper-layer thickness estimates

$$\text{i.e., } h = \frac{f_0}{g'_{3/2}} (\psi_1 - \psi_2)$$

are saved for a comparison between those observed and those from the PE model.

The spatial distribution of mean upper-layer depth for the January–December period from the eddy-resolving QG model is given in the upper panel of Fig. 4. This distribution is qualitatively similar to that given in the upper panel of Fig. 3 obtained from the 1½ layer PE model, since both maps are determined by the distribution of the mean wind-stress curl. In each case, the California Current is found to occur 250–750 km off the coast of California.

The spatial distribution of the rms variability in sea level from the eddy-resolving QG model is shown in the lower panel of Fig. 4. The QG model presents a very different spatial pattern of variability than that of the PE model (and of the observed data) shown in the lower panel of Fig. 3. Most conspicuous is the absence of strong variability along the coast, particularly between Monterey and Cape Mendocino. Rather, the dominant characteristic of the QG model reflected in the spatial distribution of rms is its ability to sustain baroclinic instability in the mean currents. This is most strongly evidenced by the presence of a zonal band of high rms variability in the southern portion of the model domain (20°–25°N). This occurs in the region of westward return flow of the subtropical gyre, where conditions for baroclinic instability are more favorable than, say, for the California Current (e.g., Lee 1988). Yet, to a lesser degree, baroclinic instability occurs in the California Current as well, evidenced by an alongshore band of maximum values of the rms differences superimposed upon the mean position of the California Current. Auad et al. (1991), using this same model, showed the highly energetic eddy fields of the coastal region (their area 1) to be fed by energy transmitted from the wind into available potential energy of the mean flow; subsequently, baroclinic instability processes transform available potential energy into eddy kinetic energy. Their analysis also showed baroclinic instability dominating barotropic instabilities in this eddy-generating process. As pointed out by Auad et al. (1991), these energy paths represent only averaged processes. The contention that baroclinic instability dominates barotropic instability or direct wind forcing does not mean that these other processes are absent.

Other sources of mesoscale variability are of course possible in the QG formulation (and the PE model)

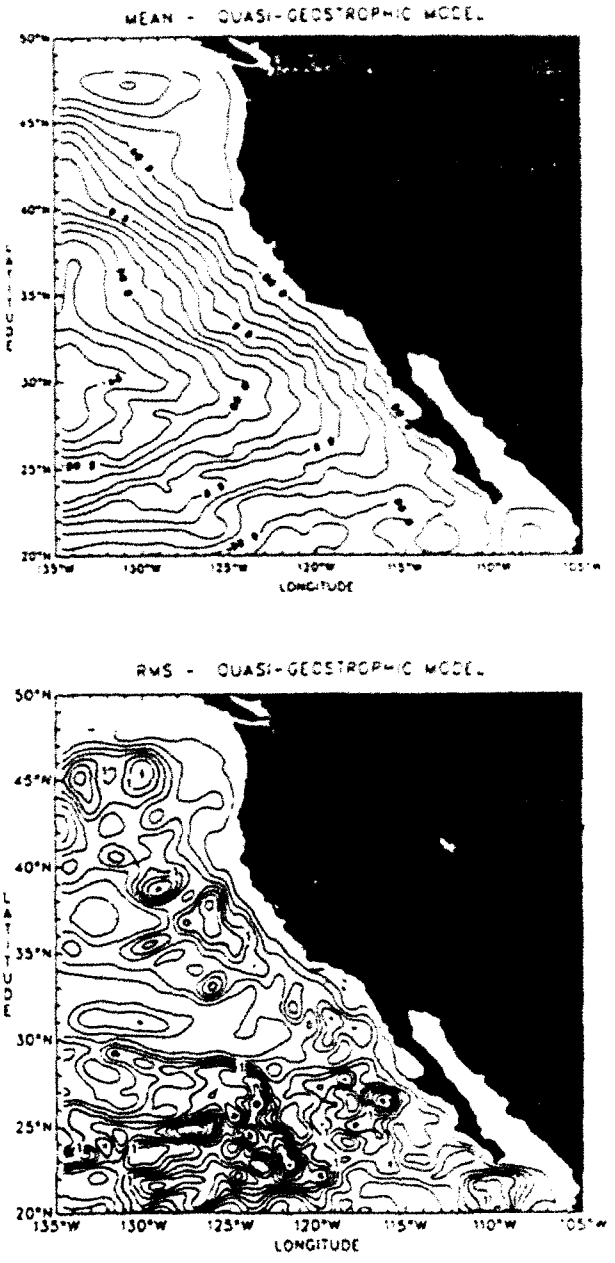

FIG. 4. (Upper panel) Spatial distribution of the mean upper-layer thickness (m) obtained from the eddy-resolving QG model for the one-year period January 1987–December 1987. The total mean has been substracted from the figure. (Lower panel) Spatial distribution of the rms residuals (cm) of the eddy-resolving QG model sea level for the one-year period January 1987–December 1987.

besides baroclinic instability. Two candidates are barotropic instability and direct wind-stress curl variability at the eastern boundary. In the study of Cummins et al. (1986) the latter mechanism provides all the variability in the model. In their work waves can clearly be seen emanating from the eastern boundary at two principal locations near the coast and propagating southwestwardly toward the far field. Although this mechanism of generation is certainly present in the QG model used here, its response is overshadowed by the effect of baroclinic instability, as demonstrated by Auad et al. (1991).

Another difference between the PE and QG model is the freedom of the former to respond to the irrotational part of the wind stress that is precluded a priori in the QG model. By decomposing the wind-stress field into an irrotational part and a nondivergent part [i.e., $\tau = \tau^I + \tau^N$, where $\nabla \times \tau^I = 0$ and $\nabla \cdot \tau^N = 0$, see Morse and Feshbach (1953)], we can quantify the contribution (not shown) of the irrotational part of the wind in the PE model. By forcing the PE model with only τ^I we find that the response in the open ocean is minimal. At the coast, although an evident seasonal cycle exists, its magnitude is negligible compared to the magnitude of the seasonal cycle produced by the nondivergent part of the wind.

The main dynamical difference between the two models is, however, the filtering of gravity waves in the QG model. As discussed below, this is the decisive factor explaining the lack of observed mesoscale variability in the coastal QG model. Moreover, it explains the inability of the QG model to simulate the observed radiation of coastal eddy energy into the ocean interior, a process that we argue is determinant in the eastern Pacific.

5. Intercomparison between observed and model RMS variability

The characteristic spatial distribution of the rms residuals in altimetric sea level displayed in Fig. 2 are compared with those of the PE and QG models displayed in Figs. 3b and 4b. As discussed earlier, maximum rms variability in observed altimetric sea level occurs adjacent to the coast of Northern California from 37°N to 40°N, coincident to the region of maximum annual variability of the wind stress (e.g., Nelson 1977). Southwest of Point Conception, a local maximum in rms variability exists; a local minimum in the rms occurs in the California Bight; and another local maximum occurs adjacent to Punta Eugenia.

To affect the comparison of the spatial distribution of the two sets, the sea-level residuals from the PE model are treated to exactly the same preprocessing filters as applied to the altimetric sea-level observations described in section 2. Also, the two datasets are taken over exactly the same time period. Upon inspection of these two spatial distributions, that from the PE model is seen to be qualitatively similar to that observed. The rms spatial distribution of the PE model displays a maximum between Monterey and Cape Mendocino, similar to that observed in both configuration and magnitude. Farther to the south, the PE model reproduces the local rms maximum observed southwest of Point Conception. Again, a local rms minimum in the California Bight separates the former maximum from the coast.

The contours of rms variability in the PE model are concentrated somewhat closer to the coast than with the observed altimetric sea level, particularly north of 35°N. This is probably due to the suppression of westward propagation of coastal disturbances north of approximately 35°N on period scales less than one year, that is, to the existence of a critical latitude (McCreary et al. 1987). In the particular PE model we are using (1½ layers), coastal variability is not allowed to propagate into the California Current north of 35°N, except on time scales exceeding one year. Mesoscale eddy activity in the model California Current north of 35°N is associated with periods that exceed one year in duration. This is only partially true in the observations, where both longer and shorter period activity is found in the California Current north of 35°N. A finer modal structure in the model is probably needed to simulate this broadened spectral band.

The spatial distribution of the rms sea-level residuals from the eddy-resolving QG model is shown in Fig. 4b. Upon inspection of observed and QG-model spatial distributions of rms (Fig. 2 and 4b), the QG model can be seen to present a very different spatial pattern of variability than is observed. Most conspicuously the QG model is unable to simulate the intense variability along the coast, particularly between Monterey and Cape Mendocino. Rather, the spatial distribution of rms variability in the QG model favors the generation of variability in the major currents that constitute the subtropical gyre (i.e., the California Current and the North Equatorial Current). This is induced by baroclinic instability processes. This pattern of variability in the observed rms variability is overshadowed by coastal seasonal variability. Moreover, the magnitude of these rms sea-level residuals in the California Current are smaller than those observed, suggesting that local baroclinic instability processes in the California Current are dominated by mesoscale eddy activity generated at the coast.

6. Coherence and phase between the observed and model sea level

Having shown that the PE model is able to simulate the spatial distribution of the rms sea-level residuals about the mean, we now examine the model's ability to simulate the phase of the dominant observed sea-level variability. Longitude–time matrices for observed and model sea-level residuals are presented at 40°N in Fig. 5 and at 30°N in Fig. 6. Each longitude–time matrix extends from the coast of California westward to

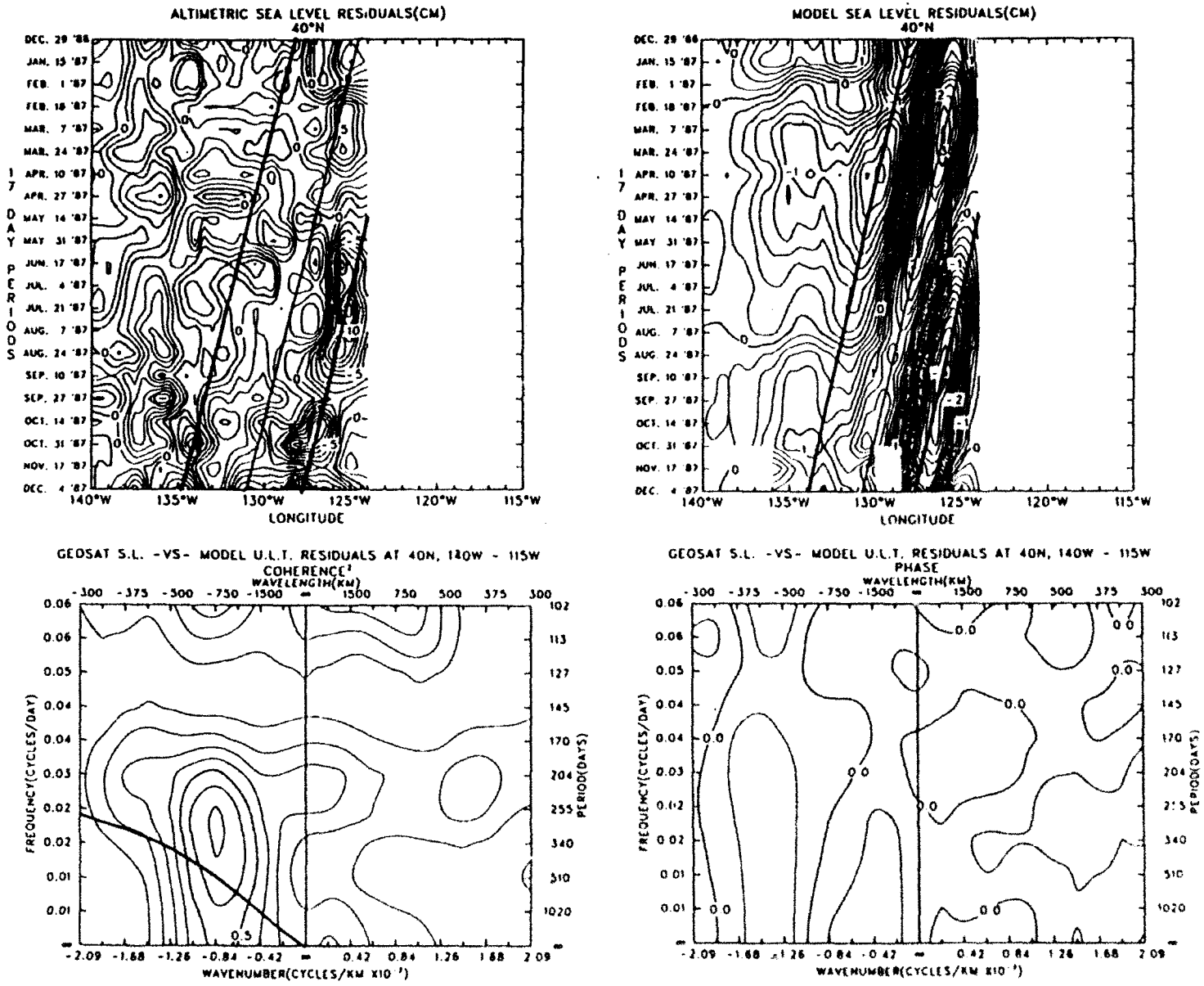

FIG. 5. (Upper panels) Longitude–time matrices of altimetric sea-level residuals, both observed (left) and from the PE model (right) at 40°N. (Middle panels) Zonal wavenumber–frequency spectra corresponding to the longitude–time matrices of the upper panel. (Lower panels) Squared coherence (left) and phase (right) between the two datasets represented in the upper panels.

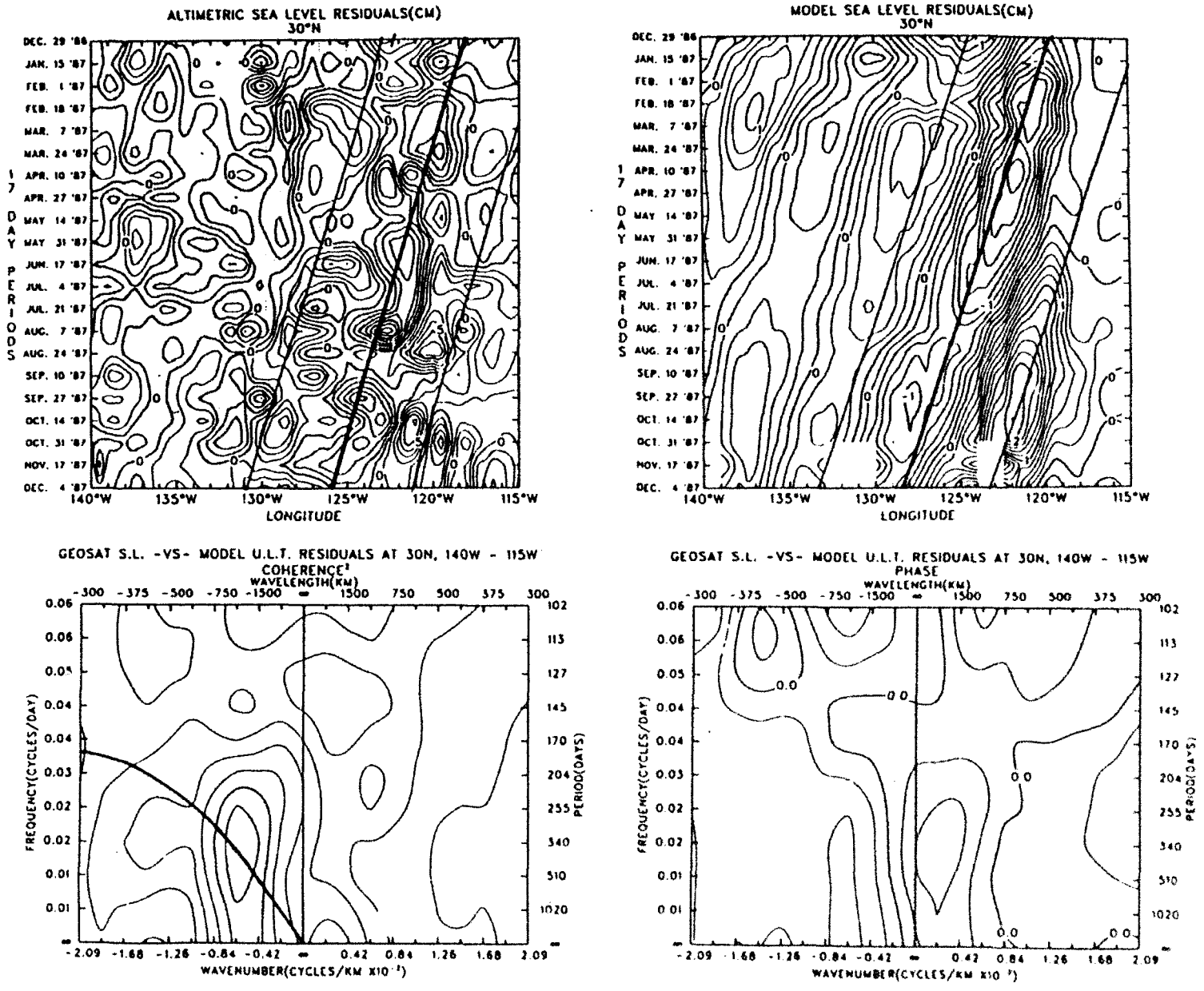

FIG. 6. Same as Fig. 6 but for latitude 30°N.

140°W for the one-year period January 1987–December 1987. The spectral coherence and phase between the two matrices at each latitude are also given.

At 40°N, both the observed and model sea-level residuals are dominated by a strong annual cycle (upper panels Fig. 5). From November to May, values are positive along the coast, indicating a downwelling regime brought on by strong poleward wind stress. After May, positive values propagate westward with negative values developing at the coast. In both matrices, the region of positive and negative residuals propagates westward from the coast as the residuals of opposite sign develop at the coast. This process is associated with Rossby wave propagation (Pares-Sierra 1991). Note, however, in both matrices this westward propagation is arrested at 250–500 km from the coast, associated with a rapid reduction in the magnitude in the offshore direction. In the PE model, this is a manifestation of the Rossby wave critical latitude, where waves of annual period generated at the coast are trapped near the coast at 40°N, this due to their strong offshore decaying factor at these periods (McCreary et al. 1987). From the good qualitative comparison between these two longitude–time matrices in the coastal waveguide, we can infer that similar dynamical processes are operating in the observed situation as well to trap eddy energy in the coastal waveguide. West of the coastal waveguide (i.e., in the California Current), both the observed and model longitude–time matrices display longer period-scale variability required to escape the coastal trapping mechanism. The observed matrix does contain higher-period mesoscale eddy activity west of the coastal waveguide, but its energy is small compared to the longer period activity that has its origins at the coast; its source could be baroclinic instability or local forcing by the time-varying wind curl.

Within the longitude–time matrices at 40°N, observed mesoscale eddy activity displays a wider range of spatial and temporal scales than in the PE model. Model sea-level residuals are heavily dominated by the annual frequency, with little influence of the higher-frequency variability that is observed. We believe this to be due to the lack of baroclinic instability in the model, possibly exacerbated by the lack of mesoscale synoptic wind-stress estimates with which to force the PE model. The differences in the patterns of spectral energy density in the zonal wavenumber-frequency domain (not shown) confirm this inability of the model to simulate the wider bandwidth of spectral response to the wind-stress forcing. For the model sea-level residuals, the spectral energy density is concentrated at frequencies lower than about 0.3 cycles/month (i.e., corresponding to periods greater than approximately 4 months). For the observed sea-level residuals, most of the spectral energy is also below 0.3 cycles/month, but above this frequency the spectrum is relatively flat, with an order of magnitude greater spectral energy density than in the PE model.

Both zonal wavenumber–frequency spectra at 40°N display peaks in their spectral energy density in the negative wavenumber quadrant near the theoretical Rossby wave dispersion curve, the latter calculated using the 1½-layer PE model characteristics. This indicates that most of the energy in both the real and model oceans propagates westward in the form of quasi-linear Rossby waves, with shorter periods adjacent to the coast and longer periods farther offshore.

Squared spectral coherence between the observed and model sea-level residual matrices at 40°N (bottom panel of Fig. 5) is significant, with squared coherence larger than 0.5 for the range 0.0 to 0.03 cycles/day and −0.5 to −0.17 cycles/degree of longitude. Therefore, at 40°N the PE model can explain more than 70% of the variance in that zonal wavenumber–frequency range. These scales of variability also dominate the zonal wavenumber–frequency spectra and provide a definition in this study for mesoscale eddy activity. Spectral phase indicates that for this range of zonal wavenumbers and periods, where high coherence exists, the model and observed signals are nearly in phase.

At 30°N, the ability of the wind-driven PE model to simulate the observed altimetric sea-level residuals (top panel in Fig. 6) is basically the same as at 40°N (Fig. 5). Significant spectral coherence occurs between the observed and model sea-level residuals over a range of frequencies that include annual and semiannual periods, with a phase difference of less than 45° (i.e., less than 1.5 months). One difference is that at these period scales, westward propagation of signals from the coast is not arrested by the influence of the critical latitude. Moreover, in agreement with linear Rossby wave theory, westward propagation of these signals from the coast is faster at 30°N than at 40°N, as characterized by a larger slope of the positive and negative contours in both longitude–time matrices in Fig. 5 compared to those in Fig. 6.

8. Discussion and conclusions

In the Introduction, we hypothesized two sources for the generation of mesoscale eddy activity in the California Current. They are local baroclinic instability of the current and/or remote generation of eddy activity by the wind stress adjacent to the coast, the latter propagating westward into (and through) the California Current via Rossby wave dynamics. In this study, two models are utilized to test the relative significance of these two sources. One model is eddy resolving and quasigeostrophic (QG), with the ability to represent baroclinic instability but not the coastal response to winds. The other model is a noneddy resolving 1½-layer primitive equation (PE), with the ability to represent the coastal response to winds but not baroclinic instability. Both models have similar spatial grids (i.e., approximately 20 km) and are driven by the same coarse-grid wind-stress forcing fields over the same one-year time period (i.e., January 1987 to December 1987). This period is chosen because of the availability

of Geosat altimetric sea-level observations with which to verify the models.

We find in this study that the PE model is able to simulate qualitatively the observed distribution of the eddy variance as it appears in altimetric sea level. It also yields significant coherence and phase between modeled and observed sea-level residuals along longitude–time matrices at 30°N and 40°N. The QG model, on the other hand, is found incapable of simulating the dominant qualitative features of the eddy variance. The reason for the agreement between the PE model and the Geosat altimetric sea-level observations is that the dominant source of mesoscale eddy activity on these time and space scales is the wind forcing adjacent to the coast. Therefore, we conclude that the wind-driven coastal generation of mesoscale eddy activity dominates that of baroclinic instability in the production of mesoscale eddy activity in the California Current.

The more significant difference between the QG model and the PE model in relation to this study is the lack of the necessary degrees of freedom of the former to sustain gravity waves [i.e., Poinaré and Kelvin waves. Ripa (1991)]. Although Poincaré waves are probably not relevant for the scales being addressed here, the filtering of Kelvin waves [by both the assumption of subinertiality (i.e., $1/\sigma f \ll 1$), as well as by the requirement of constancy of ψ (and of h) along the coast] probably suppresses a large percentage of coastally generated variability in the QG model. At least, the contribution to the mesoscale variability generated equatorward of some area of interest would be absent. This latter source has been shown to be very important at certain scales (e.g., Pares-Sierra and O'Brien 1989). Even more importantly, the QG requirement of constant layer depth along the coast very effectively buffers the response of the coastal ocean to localized wind events. Wind forcing would have to be very strong and the events would have to last long enough to lift the whole boundary at the same time.

We recognize that QG models are adequate for studying some processes in the California Current, but one of these processes is not the generation of the *total* mesoscale variability. One of its key ingredients, namely direct wind forcing of coastal variability is missing from the physics available in this model. It has been shown in this study that the eastern Pacific Ocean is not a suitable location for utilization of the QG model physics. On the other hand, if we were trying to study the dynamics of baroclinic instability in the California Current, for example, the opposite would be true; that is, the $1\frac{1}{2}$-layer PE model would be useless and the QG model would be very appropriate.

Acknowledgments. This work was supported by WESTGEC, National Institute for Global Environmental Change (Grant NIGEC/UCD No. W/GEC 91-097) and by the Consejo Nacional de Ciencia y Tecnología of México and CICESE.

APPENDIX A

Summary of Reduced-Gravity Model Parameters

Coefficient of eddy viscosity	350 m
Drag coefficient	1.5×10^{-3}
Reduced gravity	0.01 m s^{-2}
Initial upper-layer depth	200 m

APPENDIX B

Summary of Quasigeostrophic Model Parameters

Layer thicknesses (m)	100, 150, 250, 450, 650, 900, 1150, 1350
Reduced gravities (m s^{-2})	0.007061, 0.008196, 0.008389, 0.005521, 0.002170, 0.0005094, 0.00006908
Lateral friction coefficient (m^2 s^{-1})	200
f_0 (s^{-1})	7.943×10^{-5}
β (m^{-1} s^{-1})	1.92×10^{-11}
Earth's radius (m)	6.37×10^6

REFERENCES

Auad, G., A. Pares-Sierra, and G. Vallis, 1991: Circulation and energetics of a model of the California Current system. *J. Phys. Oceanogr.*, **21**, 1534–1552.

Bernstein, R. L., L. C. Breaker, and R. H. Whritner, 1977: California Current eddy formation: Ship, air and satellite results. *Science*, **195**, 353–359.

Camerlengo, A. L., and J. J. O'Brien, 1980: Open boundary conditions in rotating fluids. *J. Comput. Phys.*, **35**, 12–35.

Cummins, P. F., L. A. Mysak, and K. Hamilton, 1986: Generations of annual Rossby waves in the North Pacific by the wind-stress curl. *J. Phys. Oceanogr.*, **16**, 1979–1189.

Cummins, P., and L. Mysak, 1988: A quasigeostrophic circulation model of the Northeast Pacific. Part I: A preliminary numerical experiment. *J. Phys. Oceanogr.*, **18**, 1261–1286.

Hickey, B. M., 1979: The California current system—hypothesis and facts. *Progress in Oceanography*, Vol. 8, Pergamon, ———.

Holland, W. R., 1978: The role of mesoscale eddies in the general circulation of the ocean: Numerical experiments using a wind-driven quasigeostrophic model. *J. Phys. Oceanogr.*, **8**, 363–392.

——, 1985: Simulation of mesoscale ocean variability in midlatitude gyres. *Atmospheric and Oceanic Modeling, Advances in Geophysics*, Vol. 28A, Academic Press, ———.

——, 1986: Quasi-geostrophic modelling of the eddy-induced ocean circulation. *Advanced Physical Oceanographic Numerical Modelling*, J. J. O'Brien, Ed., D. Reidel, 203–231.

——, and L. B. Lin, 1975a: On the generation of mesoscale eddies and their contribution to the ocean general circulation. I. A preliminary numerical experiment. *J. Phys. Oceanogr.*, **5**, 642–657.

——, and ——, 1975b: On the generation of mesoscale eddies and their contribution to the ocean general circulation. Part II: A parameter study. *J. Phys. Oceanogr.*, **5**, 658–669.

——, and G. K. Vallis, 1990: An eddy-resolving model of the California Current nested in a model of the North Pacific. *J. Phys. Oceanogr.*, submitted.

Lee, D-K., 1988: A numerical study of the nonlinear stability of the eastern ocean circulation. *J. Geophys. Res.*, **93**, 10 630–10 644.

McCreary, J. P., P. K. Kundu, and S. Chao, 1987: On the dynamics of the California Current system. *J. Mar. Res.*, **45**, 1–32.

Morse, P. M., and H. Feshback, 1953: *Methods of Theoretical Physics*, McGraw-Hill, 997 pp.

Mysak, L. A., 1983: Generation of annual Rossby waves in the North Pacific. *J. Phys. Oceanogr.*, **13**, 1908–1923.

Nelson, C. S., 1977: Wind stress and wind-stress curl over the California current. NOAA Tech. Rep. NMFS SSRF-714. — pp.

Owen, R. W., 1980: Eddies of the California Current System: Physical and ecological characteristics. *The California Island: Proceedings of a Multi disciplinary Symposium*. D. Power, Ed., Santa Barbara Museum of Natural History, 237–263.

Pares-Sierra, A., 1991: Remote and local forcing of the Rossby wave variability in the midlatitude Pacific ocean. *Geofis. Int.*, 30, 121–134.

——, and J. J. O'Brien, 1989: The seasonal and interannual variability of the California Current system: A numerical model. *J. Geophys. Res.*, **94**, 3159–3180.

Rienecker, M. M., C. N. K. Mooers, and A. R. Robinson, 1987: Dynamical interpolation and forecast of the evolution of mesoscale features off the northern California. *J. Phys. Oceanogr.*, 17, 1187–1213.

Ripa, P., 1991: General stability conditions for a multi-layer model. *J. Fluid Mech.*, 222, 119–137.

Robinson, A. R., J. A. Carton, N. Pinardi, and C. N. K. Mooers, 1986: Dynamical forecasting and dynamical interpolation: An experiment in the California Current. *J. Phys. Oceanogr.*, 16, 1561–1579

Schmitz, W. J., and W. R. Holland, 1986: Observed and modeled mesoscale variability near the Gulf Stream and Kuroshio Extension. *J. Geophys. Res.*, 91, 9624–9638.

Simpson, J. J., C. J. Koblinsky, L. R. Haury, and T. D. Dickey, 1984: An offshore eddy in the California Current system. *Progress in Oceanography*, Vol. 13, Pergamon, 1–111.

White, W. B., C.-K. Tai, and J. DiMento, 1990: Annual Rossby wave characteristics in the California Current region from the GEOSAT exact repeat mission. *J. Phys. Oceanogr.*, 20, 1297–1311.

Wyllie, J. G., 1966: Geostrophic flow of the California Current at the surface and at 200 m. CALCOFI Atlas, 48 pp and 288 charts.

APRIL 1993	PARES-SIERRA ET AL	000
APRIL 1993	PARES-SIERRA ET AL.	000
APRIL 1993	PARES-SIERRA ET AL	000
APRIL 1993	PARES-SIERRA ET AL	000
APRIL 1993	PARES-SIERRA ET AL	000
APRIL 1993	PARES-SIERRA ET AL	000
APRIL 1993	PARES-SIERRA ET AL	000
APRIL 1993	PARES-SIERRA ET AL	000
APRIL 1993	PARES-SIERRA ET AL.	000
APRIL 1993	PARES-SIERRA ET AL.	000
APRIL 1993	PARES-SIERRA ET AL.	000
APRIL 1993	PARES-SIERRA ET AL.	000